

# Development of a semi-empirical potential suitable for molecular dynamics simulation of vitrification in Cu-Zr alloys

Cite as: J. Chem. Phys. **151**, 214502 (2019); <https://doi.org/10.1063/1.5131500>

Submitted: 13 October 2019 . Accepted: 13 November 2019 . Published Online: 04 December 2019

M. I. Mendelev , Y. Sun , F. Zhang, C. Z. Wang, and K. M. Ho



[View Online](#)



[Export Citation](#)



[CrossMark](#)

## ARTICLES YOU MAY BE INTERESTED IN

[Supercooled water: A polymorphic liquid with a cornucopia of behaviors](#)

The Journal of Chemical Physics **151**, 210401 (2019); <https://doi.org/10.1063/1.5135706>

[Ab initio investigation of the atomistic descriptors in the activation of small molecules on 3d transition-metal 13-atom clusters: The example of H<sub>2</sub>, CO, H<sub>2</sub>O, and CO<sub>2</sub>](#)

The Journal of Chemical Physics **151**, 214301 (2019); <https://doi.org/10.1063/1.5125769>

[Ketyl-phenoxyl triplet radical pair in glycerol: Magnetic field effect and cage kinetics in terms of the two-state model](#)

The Journal of Chemical Physics **151**, 214503 (2019); <https://doi.org/10.1063/1.5126337>



## Lock-in Amplifiers



Zurich  
Instruments

[Watch the Video](#) 

# Development of a semi-empirical potential suitable for molecular dynamics simulation of vitrification in Cu-Zr alloys

Cite as: J. Chem. Phys. 151, 214502 (2019); doi: 10.1063/1.5131500

Submitted: 13 October 2019 • Accepted: 13 November 2019 •

Published Online: 4 December 2019



M. I. Mendelev,<sup>1,a)</sup> Y. Sun,<sup>1</sup> F. Zhang,<sup>1</sup> C. Z. Wang,<sup>1</sup> and K. M. Ho<sup>1,2,3</sup>

## AFFILIATIONS

<sup>1</sup> Division of Materials Sciences and Engineering, Ames Laboratory (U.S. Department of Energy), Ames, Iowa 50011, USA

<sup>2</sup> Department of Physics, Iowa State University, Ames, Iowa 50011, USA

<sup>3</sup> Hefei National Laboratory for Physical Sciences at the Microscale and Department of Physics, University of Science and Technology of China, Hefei, Anhui 230026, China

<sup>a)</sup> Author to whom correspondence should be addressed: mendelev@ameslab.gov

## ABSTRACT

The fast increase in available computation power allowed us to decrease the cooling rate in molecular dynamics (MD) simulation of vitrification by several orders of magnitude. While the reliability of the MD simulation should obviously benefit from this increase in the computational power, in some cases, it led to unexpected results. In particular, Ryltsev *et al.* [J. Chem. Phys. **149**, 164502 (2018)] found that the most popular potentials for the Cu-Zr and Cu-Zr-Al alloys from Mendelev *et al.* [Philos. Mag. **89**, 967 (2009)] and Cheng *et al.* [Phys. Rev. Lett. **102**, 245501 (2009)] do not actually describe good glass forming systems but in contradiction with experiment predict rather fast crystallization of the Cu<sub>64.5</sub>Zr<sub>35.5</sub> alloy which is the well-known example of bulk metallic glasses. In this paper, we present a new Cu-Zr semiempirical potential suitable to simulate vitrification. No crystal nucleation was observed in MD simulation using this potential in the concentration range from 75% to 5% of Zr. Since the new potential leads to about the same liquid structure and viscosity as the Cu-Zr potential from Mendelev *et al.* [Philos. Mag. **89**, 967 (2009)] which failed to describe the good glass formability, our study clearly shows that no reliable conclusions about the glass formability can be deduced based solely on the analysis of the liquid properties and a nucleation/crystal growth study should be performed to address this question.

Published under license by AIP Publishing. <https://doi.org/10.1063/1.5131500>

## I. INTRODUCTION

Metallic glasses obtained by ultra-fast cooling of liquids can show a lot of outstanding properties.<sup>4,5</sup> However, the mechanism of vitrification is still not fully understood and numerous different approaches have been proposed (e.g., see Ref. 6). One of the problems here is that we do not really know what happens at the atomic level in a metallic alloy during the vitrification under experimental conditions. Even the state-of-the-art experimental techniques do not have a resolution allowing us to probe this extremely fast process and give us only averaged or postfactum information. A detailed information about the atomic processes governing the vitrification could be obtained from an atomistic simulation. However, the atomistic simulation in the case of glasses also faces a very difficult challenge.

Contrary to the case of crystal phases where the underlying atomic structure is known or can be predicted from the *ab initio* calculations and the properties can be obtained by perturbation of this structure, the atomic glass structure is not known. The diffraction experiments provide only averaged information like the total structure factor (TSF) (e.g., see Ref. 7). The methods to create an atomic model from this information like the reverse Monte Carlo (RMC) method<sup>8</sup> are not reliable (e.g., see Ref. 9). On the other hand, the *ab initio* molecular dynamics (AIMD) is also not reliable for the generation of a glass model by cooling a liquid because of severe time limitations of the AIMD: the typical cooling rate in the AIMD is about 10<sup>13</sup> K/s which is at least 6–7 orders of magnitude higher than a typical experimental cooling rate (10<sup>6</sup>–10<sup>7</sup> K/s). The atomic structure obtained with the AIMD cooling rate is not really a glass but more like a frozen liquid

structure (e.g., see Fig. 4 and discussion in Ref. 10). Another inherent problem associated with the AIMD simulation of the glass structure is the model size restriction (usually not more than 1000 atoms), which does not allow us to study the medium range order that in many cases determines the glass properties. The classical molecular dynamics (MD) simulation allows us to considerably relax these problems, but it relies on using semiempirical potentials of the interatomic interaction. An inadequacy of an employed semiempirical potential can easily lead to artifacts in the MD simulation. Therefore, special attention should be paid to the properties which were actually included in the potential development procedure. In this paper, we will discuss what properties should be included in the potential development procedure to simulate the vitrification in the Cu-Zr alloys.

The Cu-Zr alloys represent a rare example of binary metallic alloys which can be vitrified into bulk metallic glasses. Therefore, it is not surprising that this is one of the most studied alloys both in experiment and atomistic simulation. Two semiempirical potentials for the Cu-Zr alloys (Refs. 3 and 2) were developed about a decade ago and have been widely used since then. However, the authors of Refs. 1 and 11 showed that a rather slow cooling of the Cu<sub>64.5</sub>Zr<sub>35.5</sub> liquid alloy model described by the semiempirical potential from Ref. 2 in MD simulation leads to a nucleation of a Laves phase which grows during a subsequent high temperature annealing. A similar result was obtained for the Cu<sub>46</sub>Zr<sub>46</sub>Al<sub>8</sub> liquid alloy model described by the semiempirical potential from Ref. 3. Since even a “very slow” cooling rate in the MD simulation is several orders of magnitude higher than that in the experiment, we conclude that contrary to experimental observations, the semiempirical potentials from Refs. 2 and 3 do not describe good glass forming alloys.

This brings an important question: how to develop a semiempirical potential suitable for the simulation of vitrification? Obviously, such a potential should be fit to a liquid structure. There are several methods to accomplish this goal. The authors of Ref. 3 used the force matching method originally proposed in Ref. 12. In this method, the potential is fit to the atomic forces obtained from *ab initio* calculations performed for probe disordered (liquid) atomic configurations. However, a semiempirical potential is always an approximation and cannot exactly reproduce the “*ab initio*” forces. Fitting to this very detailed information will not necessarily make a potential better. Another approach proposed in Ref. 13 allows us to directly fit to liquid or glass partial pair correlation functions (PPCFs). The authors of Ref. 2 used a modification of this approach fitting to the X-ray total pair correlation function (TPCF) obtained from the diffraction experiment for the Cu<sub>64.5</sub>Zr<sub>35.5</sub> glass. The problem with this approach is that a TPCF is even more averaged information about the liquid structure than PPCFs themselves (recall that a binary liquid is described by 3 PPCFs) such that fitting to this information may not be sufficient to reproduce all structural features. Another problem associated with the difficulty to generate a glass model in MD simulation will be discussed in Sec. II.

In addition to the liquid structure data, both potentials were fitted to crystal phase formation energies at T = 0 obtained from *ab initio* calculations. While the authors of Ref. 2 used a very limited dataset, the authors of Ref. 3 used a much larger dataset. Yet, even the potential from Ref. 3 could not pass the test

proposed in Ref. 1. Therefore, something else should be taken into account.

The goal of the present work is to develop a new semiempirical potential for the Cu-Zr alloy which would at least pass the test proposed in Ref. 1. The rest of the paper is organized as follows. First, we will discuss the target properties which were included in the potential development procedure. Next, we will present a new potential and show that this potential does pass the test proposed in Ref. 1 in the case of the Cu<sub>64.5</sub>Zr<sub>35.5</sub> alloy. We will also present the preliminary results for the vitrification and solidification in the entire Cu-Zr composition range. Finally, we will discuss why the old potential failed to describe the good glass formality of the Cu<sub>64.5</sub>Zr<sub>35.5</sub> alloy. We will compare the properties of the liquid alloys described by the old and new potentials and show that the difference between them cannot explain the different glass formalities of the systems described by the old and new potentials. Next, we will compare the driving forces and kinetics of nucleation predicted by both potentials and show that these are the key properties which provided the good glass formability of the alloy described by the new potential.

## II. TARGET PROPERTIES

The potential developed in Ref. 2 (referred below as FS1) was fitted to the experimental values obtained for the Cu<sub>64.5</sub>Zr<sub>35.5</sub> alloy: the liquid density at T = 1500 K, the formation enthalpy at the same temperature, and the X-ray total pair correlation function of the glass of the same composition at the room temperature. In addition, it was also fit to the formation energies of five crystal phases obtained from the *ab initio* calculations at T = 0. Only one of them (B2) is actually present on the equilibrium Cu-Zr phase diagram at high temperatures.<sup>14</sup> Thus, the FS1 potential was never really designed to simulate the nucleation of the Laves phases.

In the present study, we performed *ab initio* calculations at T = 0 to determine the lowest formation energy crystal phases at the compositions where there are stoichiometric compounds in the Cu-Zr phase diagram. The details of these calculations are identical to those published in Ref. 15. We also determined the formation energies of three Cu<sub>2</sub>Zr Laves phases (see Table I), B2 and B3. The results are shown in Fig. 1. They are fully consistent with the Cu-Zr phase diagram obtained in Ref. 14 except that the *ab initio* calculations predict that the Cu<sub>5</sub>Zr phase is slightly metastable at T = 0. None of three considered that Cu<sub>2</sub>Zr Laves phases are stable according to the *ab initio* calculations.

Figure 1 also shows the results obtained using the FS1 potential. Overall, it provides reasonable values of the formation energies for the compounds which are actually present on the Cu-Zr phase diagram. The striking difference is, namely, for the Laves phases; the FS1 potential makes them very stable in contradiction to the *ab initio* data (see also Table I).

TABLE I. The formation energies (eV/atom) of the Laves phases at T = 0.

Phase	<i>Ab initio</i>	FS1	FS2
MgCu <sub>2</sub>	-0.065	-0.152	-0.134
MgNi <sub>2</sub>	-0.079	-0.151	-0.161
MgZn <sub>2</sub>	-0.116	-0.150	-0.166

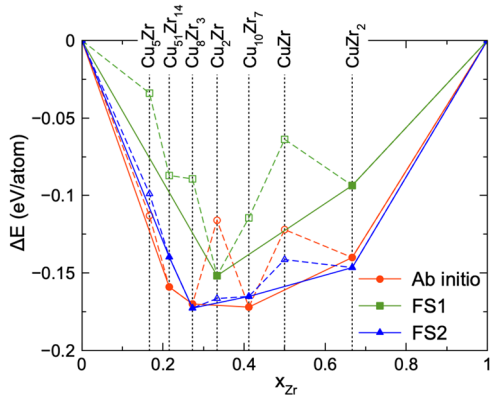


**FIG. 1.** The formation energies of the lowest energy phases for selected Cu-Zr compositions. Only the lowest energy Laves phases are shown. Open symbols and dashed lines represent metastable phases.

In order to be suitable for the simulation of solidification, a semiempirical potential should be able to also reproduce some liquid/glass properties. Three properties look like the obvious choice of target properties: atomic density, mixing enthalpy, and structure. Ideally, data for different compositions should be included; however, if the concentration dependence is not complicated, the data just for one composition around the equimolar solution should be sufficient. The authors of Ref. 2 chose to include the data for the Cu<sub>64.5</sub>Zr<sub>35.5</sub> alloy because the glass TSF, liquid density, and mixing enthalpy were obtained in experiment for this composition. In the present work, we chose to use the data for the Cu<sub>46</sub>Zr<sub>54</sub> alloy in the potential development procedure (for the reasons which will be discussed below) and used the data for the Cu<sub>64.5</sub>Zr<sub>35.5</sub> alloy for the validation of the developed potential.

The experimental value of the atomic density of the Cu<sub>64.5</sub>Zr<sub>35.5</sub> liquid alloy was reported in Ref. 2. This value was included in the potential development procedure for the FS1 potential which hence reproduces it (see Table II). The experimental mixing enthalpies for the Cu-Zr liquid alloys reported in Ref. 16 were also included in the potential development procedure in Ref. 2. As can be seen from Table II, the FS1 potential provides a reasonable prediction for the mixing enthalpy but underestimates its absolute value.

According to Ref. 2, the FS1 potential provides a very good agreement with the room temperature X-ray TSF for the Cu<sub>64.5</sub>Zr<sub>35.5</sub> amorphous alloy. However, one should be cautious regarding this statement. The point is that the glass model in Ref. 2 was obtained with a cooling rate of  $5 \times 10^{10}$  K/s which is 4 orders of magnitude higher than a typical experimental cooling rate. Since the glass structure depends on the cooling rate,<sup>10</sup> it is not obvious that this agreement would hold if the experimental cooling rate was used (in fact,

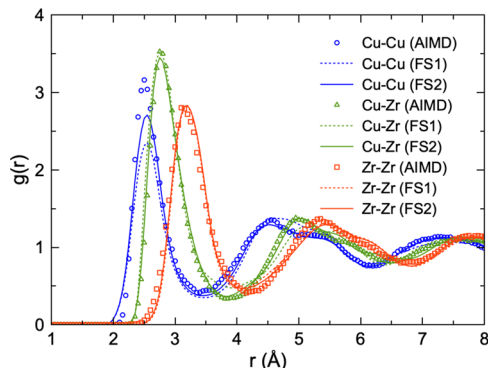


**FIG. 2.** Partial pair correlation functions of the Cu<sub>46</sub>Zr<sub>54</sub> liquid alloy at T = 1000 K.

the authors of Ref. 1 showed that it would definitely not be the case). Therefore, we performed an AIMD simulation of the Cu<sub>46</sub>Zr<sub>54</sub> liquid alloy structure at T = 1000 K. This choice of the composition was associated with the fact that the TSF for this alloy has been reported in Ref. 17 such that we could find out how well the AIMD TSF agrees with the experimental one. The choice of the temperature was associated with the fact that below T = 973 K, the experiment shows that the Cu<sub>46</sub>Zr<sub>54</sub> liquid alloy experiences some rapid ordering<sup>17</sup> which would be difficult to reproduce in the AIMD simulation because of the well-known time and size constraints. Since in the lower temperature, a larger number of structural features are seen in PPCFs, T = 1000 K, which is slightly above the transition temperature observed in experiment, looks like a reasonable choice.

The details of the AIMD simulation were identical to those in Ref. 18. The obtained PPCFs are shown in Fig. 2 along with the PPCFs obtained using the FS1 potential. The agreement overall is very reasonable taking into account that this information was not used in the development of the FS1 potential. However, there are also notable disagreements. The FS1 potential considerably underestimates the first peak of the Cu-Cu PPCF and leads to some disagreement in the second peaks of the Cu-Cu and Cu-Zr PPCFs.

In order to see if these disagreements are detectable in experiment, we compare the AIMD and FS1 X-ray TSFs with the experimental TSF in Fig. 3. Since the simulation size of an AIMD

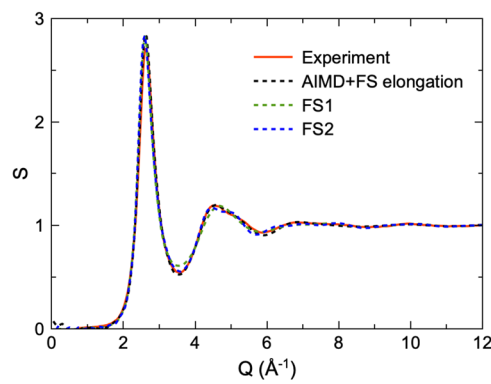


**FIG. 3.** X-ray total structure factor of the Cu<sub>46</sub>Zr<sub>54</sub> liquid alloy at T = 1000 K. The experimental data are taken from Ref. 17.

**TABLE II.** Properties of the Cu<sub>64.5</sub>Zr<sub>35.5</sub> alloy at T = 1573 K.

Property	Experiment	FS1	FS2
d (atom/nm <sup>3</sup> )	$59.2 \pm 0.3$ <sup>2</sup>	59.1	58.6
$\Delta H_m$ (eV/atom)	-0.185 <sup>16</sup>	-0.153	-0.219

**TABLE III.** Properties of the Cu<sub>46</sub>Zr<sub>54</sub> liquid alloy.

Property	Target value	FS1	FS2
d (atom/nm <sup>3</sup> ) at T = 1000 K	53.9 <sup>a</sup>	54.0	53.3
ΔH <sub>m</sub> (eV/atom) at T = 1573 K	-0.206 <sup>16</sup>	-0.149	-0.210

<sup>a</sup>This value was obtained from the AIMD simulation.

simulation model was rather limited ( $\sim 16$  Å), the PPCFs were elongated using the procedure described in Ref. 19. Figure 3 shows that the AIMD simulation provides an excellent agreement with experiment. The FS1 potential provides somewhat worse agreement in the regions of the first minimum and the second peak but better agreement in the region of the second minimum. Therefore, the FS1 potential provides about the same level of agreement with the experimental data as does the AIMD simulation.

The liquid density of the Cu<sub>46</sub>Zr<sub>54</sub> alloy obtained from the AIMD simulation is listed in Table III. While this value was not included in the potential development procedure, the FS1 potential provides an excellent agreement with the AIMD value. However, just like in the case of the Cu<sub>64.5</sub>Zr<sub>35.5</sub> liquid alloy, the FS1 potential leads to some underestimation of the mixing enthalpy of the Cu<sub>46</sub>Zr<sub>54</sub> liquid alloy.

The comparison between the target properties and the quantities predicted by the FS1 potential shows that while this potential provides reasonable predictions for most of the properties, it has an obvious deficiency associated with making the Laves phases too stable. The formation energies of all stable compounds and the mixing enthalpy of a liquid alloy can also be improved.

### III. POTENTIAL DEVELOPMENT PROCEDURE

The potential development procedure used in the present work was similar to that in Ref. 2 except for the different choice of the target properties as was described in Sec. II. The main feature of this potential development procedure is fitting to the liquid PPCFs via solution of the Born–Green–Bogoliubov equations.<sup>13</sup> In the present work, we used the Cu<sub>46</sub>Zr<sub>54</sub> liquid alloy PPCFs obtained from the AIMD simulation at  $T = 1000$  K as the target functions. The potentials for pure Cu and Zr were not changed and only the Cu–Zr pair potential was modified. The developed potential, referred below as FS2, can be found in the [supplementary material](#) and Ref. 20.

Figure 2 shows that the FS2 potential provides a better agreement with the target PPCFs than does the FS1 potential. Note that the agreement could be even better if fitting the target PPCFs was the only goal. The agreement could also be better if we refitted the Cu functions of the potential. Indeed, the FS2 potential (just like the FS1 potential) is based on the Cu1 potential developed in Ref. 21. The Cu1 potential was fit to the liquid pair correlation function obtained from the X-ray diffraction experiment. The comparison of the liquid pair correlation functions for Al obtained from the AIMD simulation and X-ray diffraction experiments shows that the AIMD tends to overestimate the first peak of the liquid pair correlation function.<sup>19</sup> While no such study was performed for Cu, the disagreement in the Cu–Cu PPCFs seen in Fig. 2 seems to be in line

with this observation. Moreover, the Cu1 potential was also fit to the Cu melting temperature. The calculation of the melting temperature from the *ab initio* calculation is a very difficult challenge and well beyond the scope of the present study. However, we note that there is no reason to *a priori* believe that the AIMD will lead to the correct melting temperature. Then, the disagreement in the liquid structure obtained from the *ab initio* and Cu1 MD simulations can be the price one should pay for providing the correct melting temperature by a semiempirical potential.

The developed potential also provides an excellent agreement with the experimental X-ray TSF (see Fig. 3), which is associated with the fact that the AIMD TSF almost coincides with the experimental one. However, the Cu<sub>46</sub>Zr<sub>54</sub> liquid alloy density is somewhat different from the AIMD value (see Table III) despite that it was included in the potential development procedure. This is again a consequence of a compromise one should make to fit all target properties. The FS2 potential provides also a worse agreement for the Cu<sub>64.5</sub>Zr<sub>35.5</sub> liquid alloy density (see Table II) comparing to the FS1 potential although the obtained value is just a little off the experimental confidential interval.

The FS2 potential provides an excellent agreement with the experimental value of the mixing enthalpy of the Cu<sub>46</sub>Zr<sub>54</sub> liquid alloy (see Table III) which was included in the potential development procedure but contrary to the FS1 potential overestimates the mixing enthalpy of the Cu<sub>64.5</sub>Zr<sub>35.5</sub> liquid alloy which was not included in the potential development procedure.

The main advantage of the FS2 potential over the FS1 potential is that it provides that all Laves phases are metastable (see Fig. 1), although it provides a worse agreement with the *ab initio* absolute value of the MgZn<sub>2</sub> Laves phase formation energy (see Table I) than does the FS1 potential. The metastability of the Laves phases was achieved by much better reproduction of other *ab initio* values of the Cu–Zr crystal phase formation energies.

Overall, based on the reproduction of the target properties, the FS2 potential should be more suitable for the MD simulation of vitrification/solidification than is the FS1 potential. In the next four sections, we present the results of the preliminary MD simulations we performed with this potential.

### IV. MOLECULAR DYNAMICS SIMULATION OF VITRIFICATION OF THE Cu<sub>64.5</sub>Zr<sub>35.5</sub> ALLOY

Since the FS1 potential failed to describe the vitrification of the Cu<sub>64.5</sub>Zr<sub>35.5</sub> alloy which is the well-known bulk glass forming alloy, we started the testing of the FS2 potential from this composition. All MD simulations described in this and the next sections were performed using the GPU-accelerated LAMMPS code.<sup>22–24</sup> The simulation cells had periodic boundary conditions in all directions and contained 5000 atoms. The short-range order (SRO) was identified using the cluster alignment (CA) method described in Refs. 25 and 26. In this method, the minimal root-mean-square deviation (RMSD) between an atomic cluster and a perfect motif is computed and the threshold to identify the short range order was set to be less than 0.15.

Figure 4 shows that the two potentials result in very similar PPCFs at  $T = 1300$  K. In the case of glass models at  $T = 300$  K obtained by cooling from  $T = 1300$  K with cooling rates of  $10^{10}$  K/s and higher, there are only slight differences in the second and third

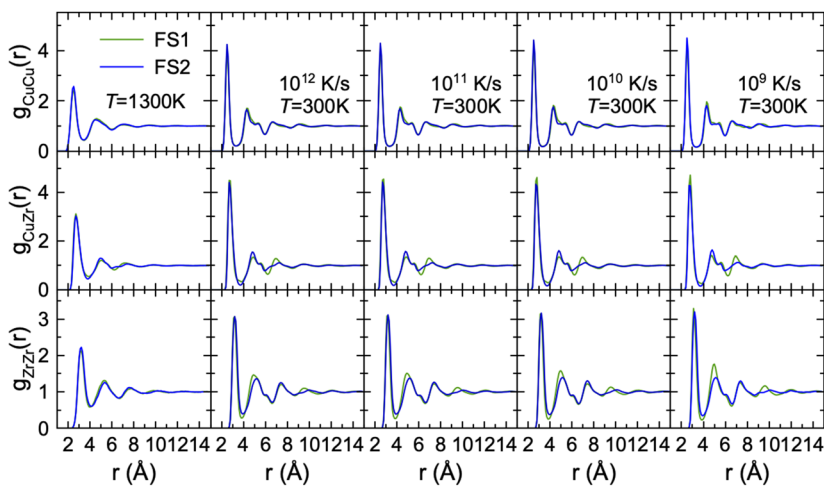


**FIG. 4.** Partial pair correlation functions of the Cu<sub>64.5</sub>Zr<sub>35.5</sub> liquid ( $T = 1300$  K) and glass ( $T = 300$  K) alloys. The latter were obtained using cooling rates ranging from  $10^{12}$  K/s to  $10^9$  K/s.

peaks of the Cu-Zr and Zr-Zr PPCFs between the two potentials. The difference in the Zr-Zr PPCF becomes much more pronounced when the cooling rate is  $10^9$  K/s. We will show below that this observation is related to the partial crystallization in the FS1 model (the same conclusion was obtained in Ref. 1).

It was previously found that the dominant SRO motifs in the Cu<sub>64.5</sub>Zr<sub>35.5</sub> glass are icosahedral ordering around Cu atoms and Frank-Kasper Z16 ordering around Zr atoms.<sup>26,27</sup> Figure 5 shows that if the cooling rate is higher than  $10^{10}$  K/s, using the FS2 potential leads to a slight increase in the icosahedral SRO of the glass model (by  $\sim 5\%$ ) and does not change the fraction of the Z16 SRO. Combining this observation with the similarity of PPCFs obtained using both potentials, we conclude that if the cooling rate is higher than  $10^{10}$  K/s, the FS1 and FS2 potentials lead to essentially the same structure of the liquid/glass Cu<sub>64.5</sub>Zr<sub>35.5</sub> alloy.

On contrary, if the cooling rate is  $10^9$  K/s, populations of both icosahedral and Z16 SROs dramatically increase and clearly are out of the high cooling rate trends when the FS1 potential is employed,

while the trends in the case of the FS2 potential do not change. The centers of Z16 polyhedra in all Laves phases form a tetrahedral network.<sup>28</sup> Therefore, one can use the tetrahedral network formed by the center of Z16-type Zr atoms as the order parameter to detect the crystallization of the Laves phase in the liquid and glass. By analyzing the networks of the center of the Z16 cluster in both FS1 and FS2 phases, we found abundant tetrahedral networks in the FS1 glass model [see Fig. 5(b)], while there are no tetrahedral networks in the glass model obtained using the FS2 potential [see Fig. 5(c)].

This subtle difference in the structure of the glass models obtained using the FS1 and FS2 potentials could be easily overlooked if the structure analysis was the only tool which was used. Although the glass model obtained using the FS1 potential by cooling the liquid alloy with the cooling rate of  $10^9$  K/s contains the tetrahedral networks formed by the Z16-type Zr atoms, it is difficult to reveal any sign of the crystalline order with a simple visual examination of the final snapshot (see Fig. 6). The difference in the Zr-Zr PPCFs at this cooling rate is probably a sign of the formation of the tetrahedral network in the FS1 glass model but this difference is small and attracts an attention only if one knows about the presence of the tetrahedral network. The actual difference between the FS1 and FS2 glass models can be clearly seen once the test proposed in Ref. 1 is performed; the temperature in the final glass models was increased up to  $T = 900$  K and NpT simulations were run at this temperature (which is above the liquid-glass transition temperature). Figure 7 demonstrates that the model obtained using the FS2 potential shows the expected behavior: the energy quickly raises and then (once the model reaches the equilibrium) does not change. The model obtained using the FS1 potential shows a quite different behavior: the energy also quickly raises but then starts to drop during a rather long time ( $\sim 100$  ns). This is associated with the fact that the crystal nuclei start to grow and the alloy crystallizes as can be seen just from a visual analysis of the final snapshot. Since the cooling rate used in our MD simulation ( $10^9$  K/s) is at least 3 orders of magnitude higher than that used in experiment, we conclude that the FS1 potential does not describe a good glass forming system. Based on the test described above, it is difficult to conclude whether the FS2 potential describes a good glass forming system, but at least, it is much more suitable for the simulation of the vitrification of the

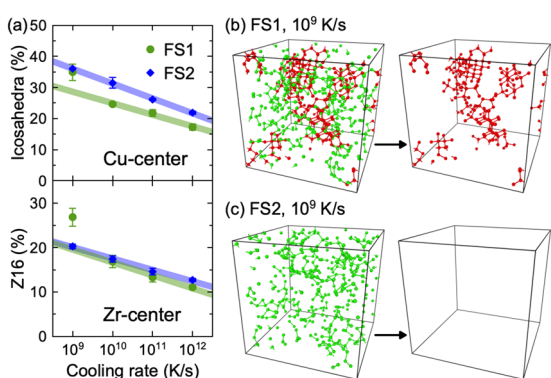


**FIG. 5.** (a) Populations of the icosahedron SRO and Z16 SRO in Cu- and Zr-centered clusters, respectively. The shadow lines indicate the trends of the SRO populations. [(b) and (c)] Networks of Z16-type Zr atoms in the glass models obtained using the FS1 and FS2 potentials, respectively. The Zr atoms forming a tetrahedron motif with its neighbor Z16-Zr are highlighted by red. The right panel only shows tetrahedron motifs.

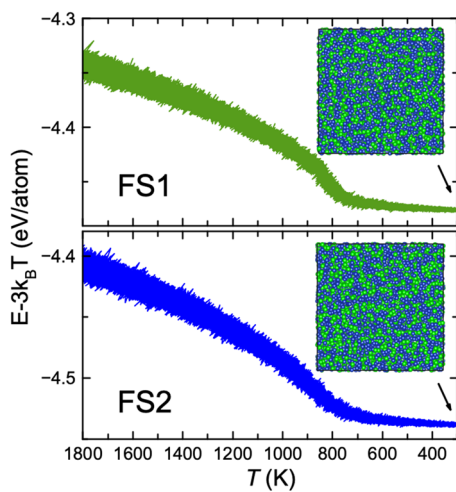


**FIG. 6.** The energy as a function of temperature during cooling from 1300 K to 300 K with the rate of  $10^9$  K/s. The final snapshots are shown. The blue is Cu atom and green is Zr.

Cu<sub>64.5</sub>Zr<sub>35.5</sub> alloy than is the FS1 potential (see further discussion in Sec. IX).

Figure 7(b) shows the energy as a function of time for the FS1 liquid model at  $T = 900$  K obtained by cooling from  $T = 1300$  K. No crystal growth is observed in this case. Therefore, the subcritical nuclei form below  $T = 900$  K but the solid-liquid interface (SLI)

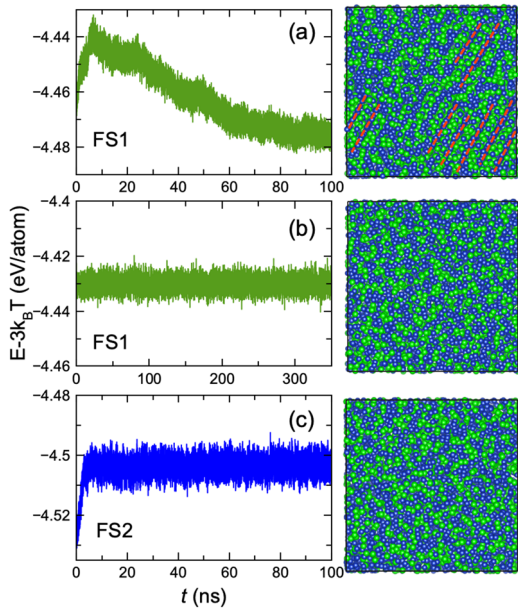


**FIG. 7.** The energy as a function of time during NpT annealing at  $T = 900$  K of (a) the heated up FS1 glass model, (b) the cooled down FS1 liquid model, and (c) the heated up FS2 glass model. The final snapshots are shown. The blue is the Cu atom and green is Zr. A clear crystalline order which is highlighted by the red dashed lines can be seen in (a).

velocity is too slow at that temperature such that they do not have enough time to grow. The authors of Ref. 1 observed nucleation at  $T = 800$  K and  $T = 850$  K when they stopped annealing and performed NpT MD simulation.

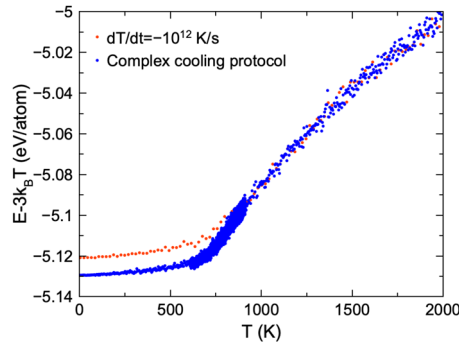
## V. MOLECULAR DYNAMICS SIMULATION OF VITRIFICATION IN Cu-Zr ALLOYS

While the main motivation for improving the Cu-Zr FS potential in the present study was the inability of the FS1 potential to describe the good glass formability of the Cu<sub>64.5</sub>Zr<sub>35.5</sub> alloy, it is important to find out if the new potential (FS2) is suitable for the MD simulation of the vitrification in the wide range of the compositions. Since using the cooling rate of  $10^9$  K/s is computationally expensive, we checked the glass formability for other compositions using a complex cooling protocol. All models contained 5000 atoms. First, we cooled down a liquid alloy from  $T = 2000$  K to  $T = 0$  with the cooling rate of  $10^{12}$  K/s. This simulation allowed us to approximately determine  $\tilde{T}_g$  from the temperature dependence of  $E - 3k_B T$  using the method described in Ref. 2. Next, we performed new cooling from the same initial liquid model at  $T = 2000$  K; however, this time, we used the following complex cooling protocol:

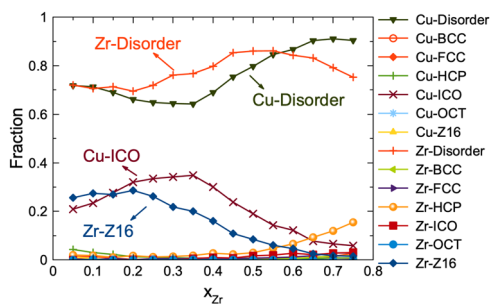
$$-\frac{dT}{dt} = \begin{cases} 10^{11} \text{ K/s if } T > \tilde{T}_g + 100 \\ 10^9 \text{ K/s if } \tilde{T}_g - 200 < T < \tilde{T}_g + 100. \\ 10^{11} \text{ K/s if } T < \tilde{T}_g - 200 \end{cases} \quad (1)$$

Figure 8 shows the energy as function of temperature obtained for the Cu<sub>45</sub>Zr<sub>55</sub> alloy as an example. One can clearly see that there is no difference between the temperature dependences of energy obtained using two cooling protocols at high temperatures. At low temperatures, the diffusion is almost suppressed (at least on the MD time scale) and there is no point to use a low cooling rate, too. The similar slopes to the temperature dependences obtained using two cooling protocols support this supposition. Therefore, the only temperature range where the cooling rate matters is around  $T_g$ . This justifies the complex cooling protocol we used.

The entire composition range of the Cu-Zr alloys was sampled with the step of 5%. Pure Cu and Zr completely crystallized even at the cooling rate of  $10^{12}$  K/s. The Cu<sub>5</sub>Zr<sub>95</sub> and Cu<sub>10</sub>Zr<sub>90</sub> alloys also crystallized at the cooling rate of  $10^{12}$  K/s. Cu<sub>15</sub>Zr<sub>85</sub> and Cu<sub>20</sub>Zr<sub>80</sub>



**FIG. 8.** The energy as a function of temperature during cooling of the liquid Cu<sub>45</sub>Zr<sub>55</sub> alloy.



**FIG. 9.** The populations of different SROs as a function of Zr composition of the glass model generated with a cooling rate of  $10^9$  K/s. Each curve corresponds to the Cu/Zr-centered clusters aligned to chosen templates (ICO: icosahedra; OCT: octahedra; Z16: Frank-Kasper Z16 polyhedra). The clusters, which could not be recognized using the chosen templates, are classified as disordered clusters.

alloys crystallized at the complex cooling protocol. The rest of the studied alloys vitrified. Thus, the addition of Zr much more strongly suppresses the crystallization of Cu than the addition of Cu suppresses the crystallization of Zr. This can be explained by the difference in the atomic sizes: Cu is much less tolerant to the larger Zr atoms than Zr is tolerant to smaller Cu atoms (see the discussion in Ref. 29). It should also be noted that Zr solidifies into the bcc lattice which easily nucleates comparing to the fcc lattice (see the discussion in Ref. 30).

Figure 9 shows the results of the application of the cluster alignment method to study the SRO in the obtained glass models at  $T = 0$ . In the Cu rich alloys, the structure is dominated by the icosahedral motif for the Cu atoms and the Z16 motif for the Zr atoms. The structural analysis did not reveal any dominant motif in the Zr rich alloys although the hcp motif around Zr atoms clearly increases with increasing Zr concentration. This increase, however, may not be related to the fact that the low temperature ground state for Zr is hcp because as we will show below, the Zr rich alloys solidify into the bcc structure.

To check if any of the obtained glass models contains crystal nuclei, we heated all of them up to  $T = 900$  K and annealed at this temperature for 100 ns. Figure 10 shows that none of these models shows any signs of crystal growth. Therefore, the FS2 potential

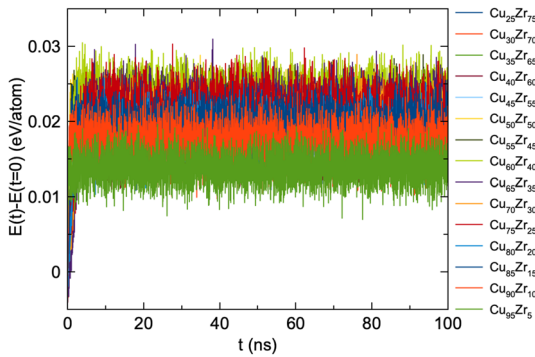


**FIG. 10.** Change of the energy during annealing the glass models at  $T = 900$  K and annealing them at this temperature.

can be used to study the vitrification in the Cu-Zr alloys in the concentration range between 5% and 75% of Zr. It should be noted that the actual concentration range where the liquid alloy vitrifies in experiment is narrower (from 30% to 70% of Zr<sup>31</sup>). This is obviously associated with the fact that the cooling rate used in our MD simulation was still at least 3 orders of magnitude higher than that in experiment.

## VI. MOLECULAR DYNAMICS SIMULATION OF SOLIDIFICATION IN CU-ZR ALLOYS

As was mentioned in Sec. V, the models with the Zr content larger than 75% solidified into a crystal structure during cooling down the liquid alloys. Despite that the dominant Zr motif in the Zr rich glass samples is hcp, all alloys with the Zr content larger than 75% solidified into the bcc structure (see Fig. 11).

The crystallization of the Cu<sub>15</sub>Zr<sub>85</sub> alloy is shown in Fig. 12. This figure shows that the liquid alloy does contain the hcp and fcc subcritical nuclei for some time. Then, a bcc nucleus emerges (at ~75 ps) and starts to grow while the hcp/fcc nuclei do not. Interestingly, a similar crystallization mechanism was observed for pure Tb in Ref. 32.

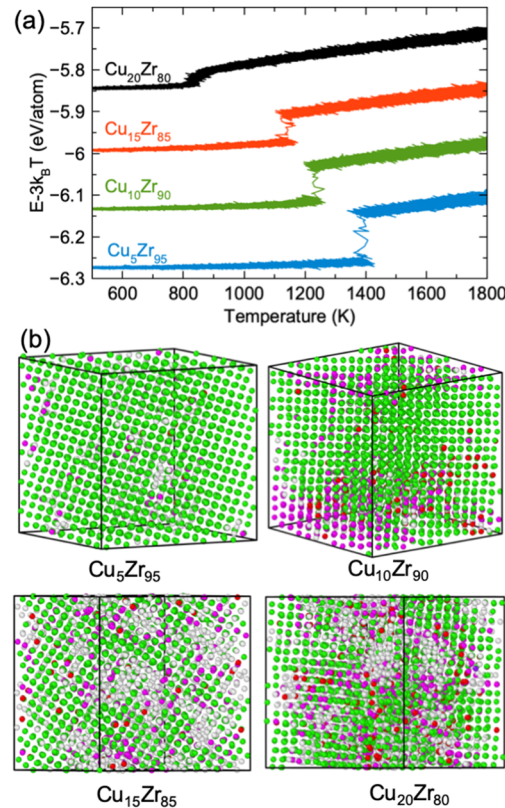


**FIG. 11.** (a) The energy as a function of temperature for the Zr-rich models cooled with a cooling rate of  $10^{10}$  K/s. (b) The snapshot of final models in (a). The local crystalline order was recognized by the cluster-alignment method. Green is bcc, pink is hcp, and red is fcc. The gray is for atoms with unrecognized local ordering (disordered).

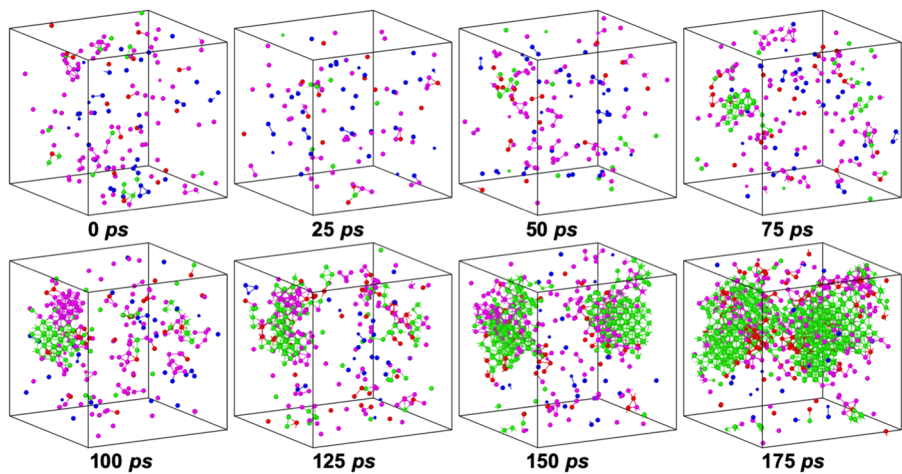


**FIG. 12.** Crystallization in the  $\text{Cu}_{15}\text{Zr}_{85}$  model cooled down with a rate of  $10^{10}$  K/s. The local crystalline order was recognized by the cluster-alignment method. Green, pink, red, and blue colors represent bcc, hcp, fcc, and icosahedral ordering, respectively.

We also note that the fraction of the Z16 which is typical for the Laves phases is slightly higher in the liquid  $\text{Cu}_{64.5}\text{Zr}_{35.5}$  alloy described by the FS2 potential than that in the same liquid alloy described by the FS1 potential. Yet, it is the liquid alloy described by the FS1 potential which crystallizes into the Laves phase during MD simulation rather than the liquid alloy described by the FS2 potential. Therefore, one cannot conclude about the nucleation ability of a liquid alloy based on the study of the dominant structural SRO motifs.

## VII. MOLECULAR DYNAMICS SIMULATION OF ATOMIC DYNAMICS IN THE $\text{Cu}_{64.5}\text{Zr}_{35.5}$ LIQUID ALLOY

The obvious difference between the FS1 and FS2 potentials is the ability to predict the Laves phase formation energies at  $T = 0$  (see Fig. 1), which is one of the reasons for their different ability

to describe the vitrification in the  $\text{Cu}_{64.5}\text{Zr}_{35.5}$  alloy as will be discussed in Sec. VIII. However, one can still wonder if this difference in the vitrification can be attributed to the difference in the liquid alloy properties. As we noted above, the FS1 and FS2 potentials lead to almost identical liquid structures (see Fig. 4), and now, we turn to the examination of kinetic properties of the  $\text{Cu}_{64.5}\text{Zr}_{35.5}$  liquid alloy obtained with these two potentials. The temperature dependence of the shear viscosity is frequently used to predict the glass formability (e.g., see Refs. 33 and 34). In the present study, we determined the shear viscosities from NVT constant number of atoms,  $N$ , volume,  $V$ , and temperature,  $T$  MD simulations via the autocorrelation functions of the stress tensor using the Green-Kubo relation,<sup>35</sup>

$$\eta = \frac{V}{k_B T} \int_0^{dt} dt \langle \sigma_{xy}(0) \sigma_{xy}(t) \rangle, \quad (2)$$

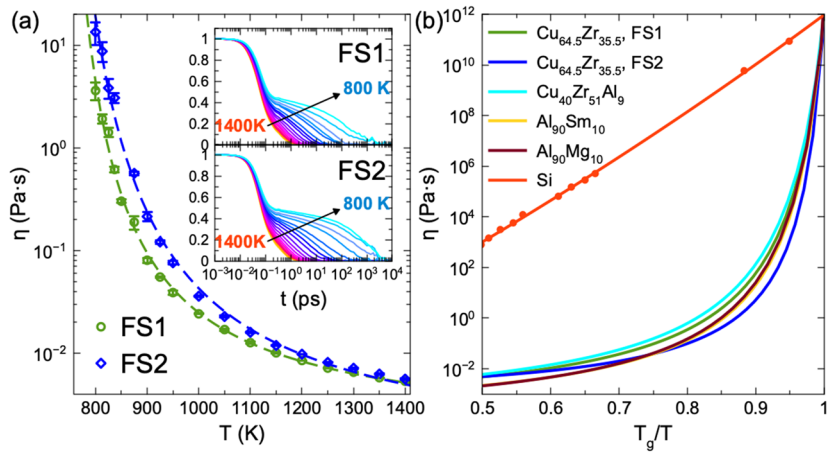


**FIG. 13.** (a) Shear viscosity as a function of temperature. The dashed lines show the interpolations obtained by fitting to the VFT equation ( $\eta = 0.016 \exp\left(\frac{-848.8}{T-693.3}\right)$ ) and  $\eta = 0.0084 \exp\left(\frac{-1292.2}{T-670.9}\right)$  for the FS1 and FS2 potentials, respectively). The upper and lower parts of the inset show normalized stress autocorrelation functions of the glass models obtained by the FS1 and FS2 potentials, respectively. The colors in this inset ranging from red to blue indicate the temperatures. (b) The Angell plot for the obtained temperature dependences of the  $\text{Cu}_{64.5}\text{Zr}_{35.5}$  alloy viscosities, as well as the simulation data for other metallic alloys from Refs. 29 and 36, and experimental data for Si from Ref. 37.

where  $\sigma_{xy}$  is the off-diagonal components of the stress tensor,  $V$  is the volume of the liquid, and  $k_B T$  is the thermal factor. The obtained temperature dependences of the shear viscosities are shown in Fig. 13(a). Both potentials lead to very similar trends: the shear relaxation is almost exponential at higher temperatures, while it becomes highly nonexponential when the system is cooled down to the lower temperatures. The obtained temperature dependences of the viscosities can be well fitted to the Volger-Fulcher-Tafmimann (VFT) equation. The liquid described by the FS1 potential is slightly more fragile than the one described by the FS2 potential. To understand the significance of such a difference, we show in Fig. 13(b) the Angell plot of the data and compare the data obtained within the present study with the data obtained for a few other models of metallic alloys with different glass-forming ability: a strong glass former Cu<sub>40</sub>Zr<sub>51</sub>Al<sub>9</sub>,<sup>36</sup> a marginal glass former Al<sub>90</sub>Sm<sub>10</sub>, a system with no glass-forming ability Al<sub>90</sub>Mg<sub>10</sub>,<sup>29</sup> as well as with the experimental data for Si.<sup>37</sup> Figure 13(b) shows that the difference between temperature dependences obtained using the FS1 and FS2 potentials does not allow itself to explain the different glass formabilities of the liquid alloys described by these potentials.

## VIII. DISCUSSION

In the present study, we modified the FS1 potential developed in Ref. 2 to be able to simulate the vitrification in the Cu<sub>64.5</sub>Zr<sub>35.5</sub> alloy. Contrary to the FS1 potential which failed to describe a good glass forming ability of this composition, the new (FS2) potential demonstrated much better glass formability such that using the state-of-the-art MD simulation methods, we could not crystallize the liquid Cu-Zr alloy in the concentration range between 5% and 75% of Zr which is in reasonable agreement with the experiment. We now turn to the discussion why these two potentials lead to such a difference in the glass formability.

Figure 1 seems to suggest an obvious explanation; the FS1 potential makes one of the Laves phases stable while the *ab initio* calculations show that it is only metastable and the FS2 potential reproduces this feature. However, in reality, this figure does not explain the difference in the glass formability. The fact that a crystal phase is metastable does not prevent it to nucleate from a liquid. For example, it is well known that the bcc phase can nucleate prior to the fcc phase in the systems where the fcc phase is the ground state (see the discussion in Ref. 30). In the case of binary alloys, a metastable phase can show up if the formation of the stable phases requires partitioning. This is the case for the Cu<sub>64.5</sub>Zr<sub>35.5</sub> alloy where the stable crystal phases are Cu<sub>8</sub>Zr<sub>3</sub> and Cu<sub>10</sub>Zr<sub>7</sub>. Nucleation of two crystalline phases of different compositions is a very unlikely event during MD simulation. Therefore, the fact whether the Laves phase is metastable or stable with a given potential should not affect its nucleation during MD simulation. Taking into account that the formation energy of the MgZn<sub>2</sub> Laves phases described by the FS2 potential is actually lower than the corresponding value obtained with the FS1 potential (see Table I), the data shown in Fig. 1 do not suggest that the liquid described by the FS2 potential should be crystallized slower than the one described by the FS1 potential.

Table II gives a clue to understanding the better glass formability of the Cu<sub>64.5</sub>Zr<sub>35.5</sub> liquid alloy described by the FS2 potential;

it leads to a larger absolute value of the formation enthalpy of the liquid alloy. This implies that the latent heats of the Laves phases described by the FS2 potential should be smaller than the corresponding values of the system described by the FS1 potential. To verify this, we determined the latent heats of all Laves phases described by both potentials using the procedure described in detail in Ref. 38. Figure 14 shows that the latent heats of the Laves phases described by the FS2 potential are indeed much smaller than those obtained using the FS1 potential. If we assume that the melting temperature scales as the latent heat, we can expect that the melting temperatures of the Laves phases described by the FS2 potential are lower than the melting temperatures of the Laves phases described by the FS1 potential.

Determination of the melting temperature in MD simulation can be very time consuming in the case of the binary phases if the SLI mobility is very slow. We found that it is the case for the Laves phases in the Cu-Zr alloys, and in the present manuscript, we will report only our preliminary results. In order to determine the SLI velocity, we used models containing a crystal phase in the middle and liquid phases in the bottom and top of the simulation cells (similarly to those described in Ref. 39). Therefore, each model had two SLIs (normal to the z-direction). The simulation cells contained 18 000–30 000 atoms and had periodic boundary conditions in the x- and y-directions. The simulation cell sizes in the x- and y-directions were chosen in accordance with the equilibrium lattice parameters at a given temperature. Also, the simulation cells had free surfaces in the z-direction. This simulation scheme automatically provides zero stresses during the SLI migration at a constant temperature. The total energy,  $E$ , was recorded during the MD simulation as a function of time and the SLI velocity,  $V$ , was determined from the slope of the  $E$  vs  $t$  curve (see Ref. 40 for details). The obtained results are shown in Fig. 15(a). Two observations immediately follow from the examination of this figure. First, as we expected, the FS2 potential leads to much lower melting temperatures than does the FS1 potential. The second observation was much less expected; the SLI migration in the system described by the FS2 potential is at least one order of magnitude slower than that in the system described by the FS1 potential at the same undercooling.

Now, we can use the classical nucleation theory (CNT) to rationalize the obtained results. The liquid-glass transition temperature for the Cu<sub>64.5</sub>Zr<sub>35.5</sub> alloy described by the FS1 potential is 770 K.<sup>2</sup> The

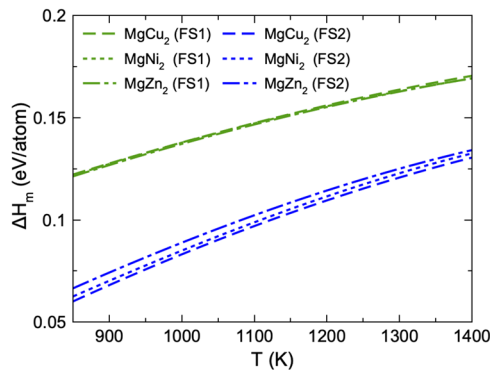
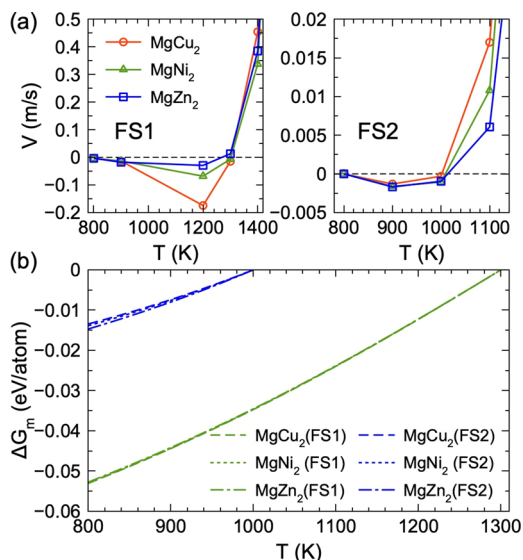


FIG. 14. The latent heat of the Laves phases.



**FIG. 15.** (a) Solid-liquid interface velocities and (b) difference in the free energy for the  $MgZn_2$  Laves phases as a function of temperature.

nucleation of the Laves phase during cooling the liquid definitely happens below  $T = 900$  K (see Fig. 7). Therefore, we will assume that it happens at  $T = 800$  K. According to the CNT, the nucleation rate can be written as<sup>41</sup>

$$J = \kappa \cdot \exp\left(-\frac{16\pi\gamma^3}{3k_B T \rho^2 \Delta G_m^2}\right), \quad (3)$$

where  $\rho$  is the atomic density,  $\gamma$  is the SLI free energy,  $\Delta G_m$  is the change in the free energy associated with melting, and

$$\kappa = \rho_L f_n^+ Z \quad (4)$$

is the kinetic prefactor, which depends on the atomic density of the liquid phase  $\rho_L$ , the rate of attachment of atoms to the critical cluster  $f_n^+$ , and the Zeldovich factor  $Z$ ,<sup>42</sup> which describes the curvature of the free energy landscape at the top of the barrier  $Z = \sqrt{|\Delta G''(n^*)|/2\pi k_B T}$ . The obtained estimations of the melting temperatures allow us to evaluate  $\Delta G_m$  using the Gibbs-Helmholtz equation (see Ref. 39 for details). Figure 15(b) shows that the change in the free energy at any given temperature is much smaller in the system described by the FS2 potential than that in the system described by the FS1 potential. At  $T = 800$  K for  $MgZn_2$ ,  $\Delta G_m = -0.0528$  eV/atom for the FS1 potential and  $\Delta G_m = -0.0147$  eV/atom for the FS2 potential.

It is much more difficult to evaluate the SLI free energy at such a large undercooling. In principle, it could be done using a persistent embryo method<sup>43</sup> and CNT as it was done for Ni-Zr B2 and B33 phases in Ref. 44. However, the kinetics of the SLI migration in the case of the FS2 potential is too slow [see Fig. 15(a)] to make any evaluation using available computational power. It should be noted that the number of studies where the SLI free energy was determined for the same binary phase using different semiempirical potentials is very limited. The authors of Ref. 45 determined the

SLI free energies of the Ni-Al and Ni-Zr B2 phases at their melting temperatures described by different semiempirical potentials. It was found that they scale approximately as  $\Delta H_m$  in agreement with the Turnbull relationship. If we assume that this relationship works at any temperature, the ratio of exponents in Eq. (3) for the FS1 and FS2 potentials is 180. However, we note that the Turnbull relation is a rather poor approximation (see the discussion in Ref. 45) and the temperature dependence of the SLI free energy can be very nontrivial (e.g., see Ref. 44).

The attachment kinetics can also play an important role (e.g., see Ref. 46). The growth kinetics for the FS2 Laves phase is so slow at  $T = 800$  K that we could not observe any interface migration during 360 ns. This is a surprising result because the difference in the driving force ( $\Delta G_m$ ) is only  $\sim 3.6$  times [see Fig. 15(b)], and we did observe the SLI migration using the FS1 potential at this temperature. It is not clear what causes such a slow SLI migration in the case of the FS2 potential. For our purpose to compare the nucleation rates, we can use the ratio of the SLI velocities at  $T = 900$  K, where we observed the SLI migration using both FS1 and FS2 potentials. At that temperature, the SLI moves approximately 10 times faster in the case of the FS1 potential. Combining these results with our estimation of the ratio of exponents in Eq. (3), we conclude that the nucleation rate in the alloy described by the FS2 potential is 3 orders of magnitude lower than that in the alloy described by the FS1 potential. Since we barely observe nucleation using the FS1 potential with the nucleation rate of  $10^9$  K/s, it explains why we never observe any nucleation using the FS2 potential.

The estimation above suggests that it is safe to use the FS2 potential in the simulation of the  $Cu_{64.5}Zr_{35.5}$  glass structure if the cooling rate is higher than  $10^6$  K/s. At the present moment, this is well below any cooling rate which was ever used in MD simulation. Of course, this estimation was made based on several approximations we had adopted to use the CNT (e.g., the Turnbull relation for the estimation of the temperature dependence of the SLI free energy). Therefore, one should be cautious applying the FS2 potential if the cooling rate is below  $10^9$  K/s and perform the detailed analysis of the final glass model structure like we performed in the present study (see also Ref. 47). The acceptable cooling rate for other compositions should be evaluated in future MD simulations.

Figures 4 and 5(a) show that the FS1 and FS2 potentials lead to similar glass structures as long as no nucleation happens (that is, the cooling rate is above  $10^9$  K/s). Therefore, glass properties obtained with the FS1 potential should be realistic (for the cooling rate used to prepare the glass model!). It is only when a nucleation happens, glass properties described by the FS1 potential may be viewed as artifacts of the MD simulation.

## IX. CONCLUSIONS

A semiempirical potential to simulate the vitrification/solidification in the Cu-Zr alloys was developed. No crystal nucleation was observed in MD simulation using this potential in the concentration range from 75% to 5% of Zr, which is in reasonable agreement with the experimental observations taking into account the difference between the cooling rates in MD simulation and experiment. Since the new potential leads to about the same

liquid structure and viscosity as the Cu-Zr potential from Ref. 2, which failed to describe the good glass formability, our study clearly shows that no reliable conclusions about the glass formability can be deduced based solely on the analysis of the liquid properties and a nucleation/crystal growth study should be performed to address this question.

Our study of the solidification in the Zr-rich alloys also vividly demonstrates that the dominant motif in the liquid structure may not be related to the crystal phase which will nucleate from the liquid alloy.

## SUPPLEMENTARY MATERIAL

See the [supplementary material](#) for the developed EAM potential in the LAMMPS<sup>48</sup> format.

## ACKNOWLEDGMENTS

This work was supported by the U.S. Department of Energy (DOE), Office of Science, Basic Energy Sciences, Materials Science and Engineering Division. The research was performed at the Ames Laboratory, which is operated for the U.S. DOE by Iowa State University under Contract No. DE-AC02-07CH11358.

## REFERENCES

- <sup>1</sup>R. E. Ryltsev, B. A. Klumov, N. M. Chtchelkatchev, and K. Y. Shunyaev, *J. Chem. Phys.* **149**, 164502 (2018).
- <sup>2</sup>M. I. Mendelev, M. J. Kramer, R. T. Ott, D. J. Sordelet, D. Yagodin, and P. Popel, *Philos. Mag.* **89**, 967 (2009).
- <sup>3</sup>Y. Q. Cheng, E. Ma, and H. W. Sheng, *Phys. Rev. Lett.* **102**, 245501 (2009).
- <sup>4</sup>A. Inoue, *Acta Mater.* **48**, 279 (2000).
- <sup>5</sup>M. M. Trexler and N. N. Thadhani, *Prog. Mater. Sci.* **55**, 759 (2010).
- <sup>6</sup>C. P. Royall and S. R. Williams, *Phys. Rep.* **560**, 1 (2015).
- <sup>7</sup>Y. Waseda, *The Structure of Non-Crystalline Materials: Liquids and Amorphous Solids* (McGraw-Hill International Book Co., New York, London, 1980).
- <sup>8</sup>R. L. McGreevy and L. Puszta, *Mol. Simul.* **1**, 359 (1988).
- <sup>9</sup>M. I. Mendelev and M. J. Kramer, *J. Appl. Phys.* **107**, 073505 (2010).
- <sup>10</sup>Y. Zhang, F. Zhang, C. Z. Wang, M. I. Mendelev, M. J. Kramer, and K. M. Ho, *Phys. Rev. B* **91**, 064105 (2015).
- <sup>11</sup>R. E. Ryltsev, B. A. Klumov, N. M. Chtchelkatchev, and K. Y. Shunyaev, *J. Chem. Phys.* **145**, 034506 (2016).
- <sup>12</sup>F. Ercolessi and J. B. Adams, *Europhys. Lett.* **26**, 583 (1994).
- <sup>13</sup>M. I. Mendelev and D. J. Srolovitz, *Phys. Rev. B* **66**, 014205 (2002).
- <sup>14</sup>M. A. Turchanin, P. G. Agraval, and A. R. Abdulov, *Powder Metall. Met. Ceram.* **47**, 428 (2008).
- <sup>15</sup>F. Zhang, M. Ji, X. W. Fang, Y. Sun, C. Z. Wang, M. I. Mendelev, M. J. Kramer, R. E. Napolitano, and K. M. Ho, *Acta Mater.* **81**, 337 (2014).
- <sup>16</sup>A. A. Turchanin, I. A. Tomilin, M. A. Turchanin, I. V. Belokonenko, and P. G. Agraval, *J. Non-Cryst. Solids* **250**, 582 (1999).
- <sup>17</sup>V. Wessels *et al.*, *Phys. Rev. B* **83**, 094116 (2011).
- <sup>18</sup>Y. Zhang, R. Ashcraft, M. I. Mendelev, C. Z. Wang, and K. F. Kelton, *J. Chem. Phys.* **145**, 204505 (2016).
- <sup>19</sup>M. J. Kramer, M. I. Mendelev, and M. Asta, *Philos. Mag.* **94**, 1876 (2014).
- <sup>20</sup>See <http://www.ctcms.nist.gov/potentials> for the Cu-Zr potential with the reference on the present paper.
- <sup>21</sup>M. I. Mendelev, M. J. Kramer, C. A. Becker, and M. Asta, *Philos. Mag.* **88**, 1723 (2008).
- <sup>22</sup>W. M. Brown, A. Kohlmeyer, S. J. Plimpton, and A. N. Tharrington, *Comput. Phys. Commun.* **183**, 449 (2012).
- <sup>23</sup>W. M. Brown, P. Wang, S. J. Plimpton, and A. N. Tharrington, *Comput. Phys. Commun.* **182**, 898 (2011).
- <sup>24</sup>W. M. Brown and M. Yamada, *Comput. Phys. Commun.* **184**, 2785 (2013).
- <sup>25</sup>X. W. Fang, C. Z. Wang, Y. X. Yao, Z. J. Ding, and K. M. Ho, *Phys. Rev. B* **82**, 184204 (2010).
- <sup>26</sup>Y. Sun *et al.*, *Sci. Rep.* **6**, 23734 (2016).
- <sup>27</sup>J. Ding, Y. Q. Cheng, and E. Ma, *Acta Mater.* **69**, 343 (2014).
- <sup>28</sup>A. Travesset, *Phys. Rev. Lett.* **119**, 115701 (2017).
- <sup>29</sup>Y. Sun, F. Zhang, L. Yang, H. J. Song, M. I. Mendelev, C. Z. Wang, and K. M. Ho, *Phys. Rev. Mater.* **3**, 023404 (2019).
- <sup>30</sup>S. R. Wilson and M. I. Mendelev, *J. Chem. Phys.* **144**, 144707 (2016).
- <sup>31</sup>M. I. Mendelev *et al.*, *Philos. Mag.* **90**, 3795 (2010).
- <sup>32</sup>H. Song and M. I. Mendelev, *J. Chem. Phys.* **149**, 244501 (2018).
- <sup>33</sup>O. N. Senkov, *Phys. Rev. B* **76**, 104202 (2007).
- <sup>34</sup>H. Tanaka, *J. Non-Cryst. Solids* **351**, 678 (2005).
- <sup>35</sup>M. P. Allen and D. J. Tildesley, *Computer Simulation of Liquids*, 2nd ed. (Oxford University Press, Oxford, United Kingdom, 2017).
- <sup>36</sup>A. Jaiswal, T. Egami, and Y. Zhang, *Phys. Rev. B* **91**, 134204 (2015).
- <sup>37</sup>C. A. Angell, *MRS Bull.* **33**, 544 (2008).
- <sup>38</sup>M. I. Mendelev, T. L. Underwood, and G. J. Ackland, *J. Chem. Phys.* **145**, 154102 (2016).
- <sup>39</sup>M. I. Mendelev, F. Zhang, H. Song, Y. Sun, C. Z. Wang, and K. M. Ho, *J. Chem. Phys.* **148**, 214705 (2018).
- <sup>40</sup>M. I. Mendelev, M. J. Rahman, J. J. Hoyt, and M. Asta, *Modell. Simul. Mater. Sci. Eng.* **18**, 074002 (2010).
- <sup>41</sup>D. Kashchiev, *Nucleation: Basic Theory with Applications* (Butterworth-Heinemann, London, 2000).
- <sup>42</sup>J. B. Zeldovich, *Acta Physicochim. (URSS)* **18**, 1–22 (1943).
- <sup>43</sup>Y. Sun, H. J. Song, F. Zhang, L. Yang, Z. Ye, M. I. Mendelev, C. Z. Wang, and K. M. Ho, *Phys. Rev. Lett.* **120**, 085703 (2018).
- <sup>44</sup>Y. Sun, F. Zhang, H. J. Song, M. I. Mendelev, C. Z. Wang, and K. M. Ho, *J. Phys. Chem. C* **123**, 6685 (2019).
- <sup>45</sup>S. R. Wilson, K. Gunawardana, and M. I. Mendelev, *J. Chem. Phys.* **142**, 134705 (2015).
- <sup>46</sup>H. Song, Y. Sun, F. Zhang, C. Z. Wang, K. M. Ho, and M. I. Mendelev, *Phys. Rev. Mater.* **2**, 023401 (2018).
- <sup>47</sup>R. E. Ryltsev, *J. Cryst. Growth* (submitted).
- <sup>48</sup>S. Plimpton, *J. Comput. Phys.* **117**, 1 (1995).